Available online at www.sciencedirect.com
ScienceDirect
International Journal of Heat and Mass Transfer 51 (2008) 273–282
International Journal of HEAT and MASS TRANSFER
www.elsevier.com/locate/ijhmt

Dynamic characteristics of transient boiling on a square platinum microheater under millisecond pulsed heating

J. Li [a], G.P. Peterson [a,*], P. Cheng [b]

[a] Department of Mechanical Engineering, University of Colorado, Boulder, CO 80309, United States
[b] School of Mechanical and Power Engineering, Shanghai Jiaotong University, Shanghai 200030, PR China

Received 3 August 2006; received in revised form 30 March 2007
Available online 15 June 2007

Abstract

A series of experimental investigations of boiling incipience and bubble dynamics of water under pulsed heating conditions for various pulse durations ranging from 1 ms to 100 ms were conducted. Using a very smooth square platinum microheater, 100 μm on a side, and a high-speed digital camera, the boiling incipience was observed and investigated as a function of the bulk temperature of the microheater, pulse power level, and pulse duration. Given a specific pulse duration, for low pulse power levels, there would be no bubble nucleation or bubble mergence, for moderate pulse power levels, individual bubbles generated on the heater merged to form a single large bubble, while for high pulse power levels, the rapid growth of the individual bubbles and subsequent bubble interaction, resulted in a reduction in bubble coalescence into a single larger bubble, referred to as *bubble splash*. The transient heat flux range at which bubble coalescence occurs was identified experimentally, along with the temporal variations of bubble size, bubble interface velocity and interface acceleration.

Keywords: Kinetics of boiling; Boiling incipience; Bubble dynamics; Explosive boiling; Pulsed heating; Microheater

1. Introduction

Pulsed heating and the associated nucleate bubble generation have been successfully used in a number of applications including thermal ink jet printers [1], bubble actuated pumps [2,3], microarray fabrication [4], bubble actuated micro-mixers [5], bio-actuators [6], medical imaging [7], DNA hybrid enhancement techniques [8], fuel injection [9] and numerous other applications at micro-length scales [10]. The fundamental mechanism used in these applications is the rapid bubble formation and growth on a small microheater, which results in a driving force that can induce the flow of the liquid. In principle, classical nucleation theory can be used to predict the boiling incipience on these microheaters and classical bubble dynamics can be used to predict the bubble behavior after the initial formation.

Asai [1], who was one of the first to study bubble dynamics on microheaters under microsecond pulsed heating conditions, developed a detailed dynamic model to predict bubble growth and collapse. Iida et al. [11] experimentally determined bubble formation and bubble nucleation rates, utilizing fast transient visualization techniques, while Avedisian et al. [12] and Thomas et al. [13] measured the nucleation threshold as a function of variations in the measured temperature for microsecond pulses. Zhao et al. [14] investigated the pressure and power generated from explosive boiling in printer heads. Yin et al. [15] studied the boiling phenomena and bubble dynamics on a serpentine, 260 μm square microheater under millisecond pulsed heating. Deng et al. [16] investigated the boiling

* Corresponding author. Tel.: +1 303 492 8908; fax: +1 303 492 8866.
E-mail addresses: dr.jimli@gmail.com (J. Li), Bud.Peterson@colorado.edu (G.P. Peterson), pingcheng@sjtu.edu.cn (P. Cheng).

0017-9310/$ - see front matter © 2007 Elsevier Ltd. All rights reserved.
doi:10.1016/j.ijheatmasstransfer.2007.03.045

Nomenclature

C_g	solubility of dissolved gas
C_P	specific heat of platinum
e_R	electrical resistivity
h	Prantle constant
h_{fg}	heat of evaporation
J	bubble nuclei density
k	Boltzmann constant
K_h	Henry's constant
N_0	molecule number per unit volume
q	heat flux
$\dot{Q}$	power
R	resistance; radius of bubble
$\dot{R}$	interface velocity of bubble
$\ddot{R}$	interface acceleration of bubble
t	time
T	temperature

Greek symbols

θ	contact angle; thermal coefficient of resistivity
σ	surface tension
λ	thermal conductivity of platinum
μ	dynamic viscosity
υ	kinetic viscosity
ρ	density of platinum
τ_P	pulse duration

Subscripts

l	liquid
v	vapor

phenomena and bubble dynamics on a very small line microheater, 0.5 μm in width, under millisecond pulsed heating. More recently, Li and Peterson [17] conducted an experimental analysis on the bubble nucleation and bubble dynamics on a smooth square microheater for pulsed heating in the millisecond range. The process of bubble growth and collapse during millisecond pulsed heating has indicated that bubble collapse can be significantly influenced by the pulse duration and power level and that there exists a sudden bubble shrinkage immediately following the pulsed heating [16,17].

As a result of the growing number of potential applications, the boiling phenomena resulting from microheaters subjected to either micro or millisecond pulse heating are of increasing interest. The previous review of recent research indicates that there is currently insufficient understanding of these phenomena to direct the design of MEMS-based devices. A better understanding of both boiling nucleation and the associated bubble dynamics occurring on microheaters, is critical to the design and operation of these devices. This will require information on how the pulse power level and duration are related to the maximum bubble radius, bubble life, and bubble behavior. An investigation of the bubble nucleation and bubble dynamics on a 100 μm square platinum heater with a very smooth surface (average roughness of 50 Å) fabricated on a Pyrex wafer was conducted. After the initial calibration of the microheater, a series of experiments was conducted to explore the boiling incipience and the bubble dynamics for millisecond pulse heating, using a high-speed CCD digital camera. The principal objectives of this investigation are to provide detailed information on bubble growth and collapse under various heating scenarios; to examine the maximum bubble radius as a function of the pulse duration and power level; and to determine the power levels and duration range at which bubble actuation in MEMS applications are feasible.

2. Experimental system

The microheater used in the current investigation was 100 μm square and 1700 Å thick, as illustrated in Fig. 1 and the detailed fabrication information can be found in Ref. [17]. Table 1 illustrates the properties of all of the materials utilized in the experimental investigation. The average roughness of the microheater surface was approximately 50 Å (5 nm) measured by using a surface scanning profilometer. This roughness is in the range of the critical bubble size for homogeneous bubble nucleation and, as such, helps to minimize the influence of cavity size on bubble nucleation.

The temperature of the microheater can be obtained from the relationship between the resistance and the temperature. The detailed calibration process of the relationship between the resistance and temperature of the microheater was also described in Ref. [17]. With the calibration and the curve fit, the resistance of the microheater, R_{heater}, was linearly related to the temperature as

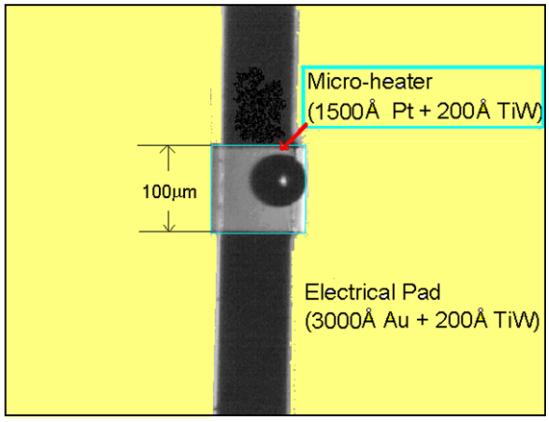

Fig. 1. The fabricated microheater.

Table 1
Properties of materials at atmospheric conditions

	e_R (Ω m)	λ (W/m °C)	C_P (J/kg °C)	ρ (kg/m^3)
Platinum	1.06×10^{-7}	71.4	133	21,460
Gold	2.45×10^{-8}	310.0	128	19,280
Water	$>0.5 \times 10^{8}$	0.6	4188	980
Pyrex glass	10^{10}–10^{14}	1.4	740	2190

$R_{heater}\,(T_{heater}) = R_0 \cdot f(R_{heater}(t)) = 1.6231 \cdot (1 + 0.002319 \times T_{heater,bulk})$.

The experimental test facility utilized in this investigation is illustrated in Fig. 2. A DC power supply (Agilent E3620A) was used to provide the high power voltage through an amplifying circuit connected to a waveform generator (Agilent 33220A), which provided the primary and trigger pulses. Completing the circuit was a reference resistance circuit composed of four 10 Ω precision resistors, which was used for the current measurement. The voltage drop in the reference resistance circuit and the microheater was recorded using a digital oscilloscope (Tektronix TD2014) with a sampling rate of at least 1.0 GS/s with the results stored in the system microcomputer.

An optical microscope (500×, Olympus BXFMF) coupled with a high-speed digital camera (Redlake MotionScope PCI 2000S) with a maximum recording rate of 2000 fps, was used to record bubble formation and behavior.

The voltage pulse from the external trigger port of the waveform generator was the primary trigger source, which was synchronized with the output pulse. As shown in Fig. 2, when the trigger pulse was sent to a CCD high-speed camera, the oscilloscope was simultaneously triggered by the amplified output pulse, which was exerted on the heating element, thus all of the equipment was triggered at the same time. In this way, the data acquisition process was highly synchronized with the heating pulse.

The test section included a Pyrex Petri reservoir and a diced Pyrex wafer with the microheater fabricated on the surface, all of which were thoroughly cleaned with acetone and rinsed with distilled water prior to each of the experiments.

The manufacturer data sheets (MDS) for the precision resistors used for current measurement, indicated a temperature coefficient (TCR) of ±20 ppm/°C, which, when compared to the TCR of standard platinum (3850 ppm/°C), resulted in a variation in the resistance during electrical heating that was negligible. The configuration of the voltage drop measurement on these resistance elements is also

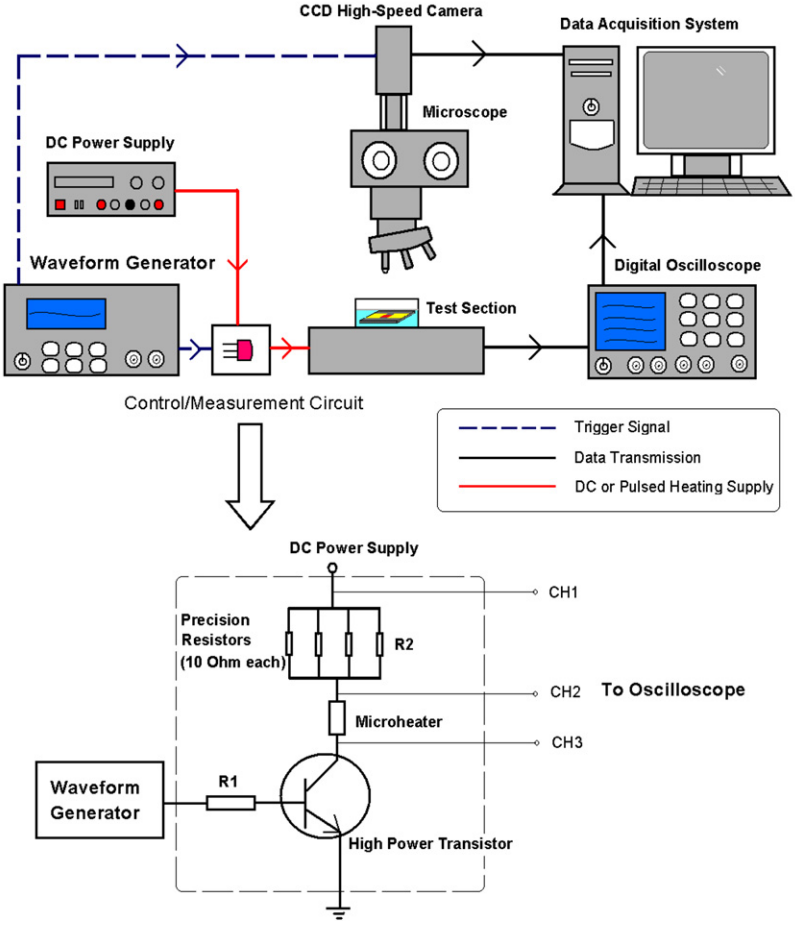

Fig. 2. Experimental setup and the resistance measurement circuit.

shown in Fig. 2. To complete the circuit, the tips of the digital oscilloscope probes were attached immediately adjacent to the resistor pins and the microheater, in order to reduce the uncertainty of the measurements.

Distilled but not degassed water was utilized as the working fluid in this experimental investigation. The bulk fluid temperature was approximately 25.0 ± 2.0 °C. (The ambient pressure was 1 atm, resulting in a sub-cooling of approximately 75 °C.) The liquid was maintained at 5 mm above the microheater to avoid the influence of the surface on the bubble behavior, as is the case for pool boiling. During all of the experiments, a slow, incremented series of voltage pulses with a fixed pulse duration (1–100 ms) were applied with 0.2 V increment between each series.

3. Uncertainty analysis

As part of the experimental procedure, the repeatability of the temperature measurements was determined by repeating the test six times for each pulse setting (three times with a large time resolution and three times with a fine time resolution). The resulting variation for the measured temperature with the measured voltage drops, statistically calculated from three repeated tests for each pulse setting, was found to be less than $\pm 6\%$ for the low pulse power levels and less than $\pm 10\%$ for the high pulse power levels. This uncertainty in the experiments is primarily due to the system, e.g., the measurement circuit, the possible residual thermal stresses of the microheater resulting from the microfabrication processes and the condition of the bulk liquid. Any noise from the environment will influence the equipment and the electrical circuit, and any variations in the bulk temperature of the liquid may also result in some uncertainty in the voltage measurements. The uncertainty in the power measurement using the measured voltage drops on the different elements, was determined to be less than $\pm 5\%$. The uncertainty in the bubble radius determination was less than ± 0.2 μm at the maximum data processing rate with the high-speed digital camera software (240×92 pixels each frame for 2000 fps).

It should be noted that for a square heater driven by the Joule heating from an electrical current, the temperature distribution in the microheater is not uniform, but hottest in the center and cooler at the overlap between the microheater and the connection pads. In our previous work [17], we have thoroughly analyzed the difference between the measured averaged bulk temperature of the microheater and the highest possible temperature in the microheater using a transient 3D conduction model concerning the Joule heating inside the connection pads and the microheater. For a heating pulse of 120 ms and 0.117 W, the magnitude of this difference is about 25 °C [17]. The present measurement of the average bulk temperature can be used as a reference temperature for boiling incipience. One can use this bulk temperature and other experimental parameters to obtain a more accurate temperature distribution in the microheater through a detailed 3D transient numerical model, but this kind of work is beyond the present research.

4. Experimental results and discussion

As previously stated, the principal objective of the current investigation was to provide detailed information on bubble growth and collapse under various heating scenarios; to examine the maximum bubble radius as a function of the pulse duration and power level; and to determine the pulse power level and duration ranges at which bubble actuation in MEMS applications is feasible. In the following section, bubble nucleation and bubble dynamics under different heating pulse durations and power levels are explored and discussed in detail.

Fig. 3 shows three typical processes of bubble nucleation, bubble growth and collapse under different pulse heating scenarios. Fig. 3a illustrates bubble nucleation and growth on a smooth surface in distilled water for a 100 ms heating pulse with an average pulse power level of 0.18 W. As shown, the rate of bubble growth after bubble nucleation (28 ms) was quite large, and very shortly after the application of the heating pulse the bubble shrank rapidly (103 ms). Figs. 3b and c show similar results for 10 ms (0.28 W), 5 ms (0.33 W) pulse durations and levels, respectively.

A typical time-synchronized, measured temperature variation for a 10 ms pulse is presented in Fig. 4. It is important to note here that because the temperature was measured using an electrical resistance technique and there is no current immediately preceding or following the application of the heating pulse, thus there is no temperature measurement immediately before and after the pulse. The local maximum point or the turn point (as similar to the inflection point as discussed by Avedisian et al. [12] and Thomas et al. [13]), as shown in Fig. 4, indicates the onset of the bubble nucleation on the heater surface. The onset of visible bubble nucleation as observed using the optical microscope, coupled with a high-speed digital camera and a maximum recording rate of 2000 fps, is identified by the arrow as shown in Fig. 4, which marks the onset of bubble coalescence.

Fig. 5 presents the boiling incipience temperature from the inflection point of the temperature variation curve for different heating pulse durations. As indicated, the incipience temperature is closely related to the pulse duration, such that the shorter the pulse duration, the higher the incipience temperature. Only the results from the moderate pulse power levels are presented here. Higher pulse power levels will result in slightly higher incipience temperatures, but those tests with much higher power levels were not conducted, due to the high probability of heater burnout. As discussed previously, in order to reduce the uncertainty of the experimental results, the data illustrated in Fig. 5 represents the average value from three separate tests for each given pulse power level and duration. The dashed line shown in Fig. 5 represents the theoretical nucleation

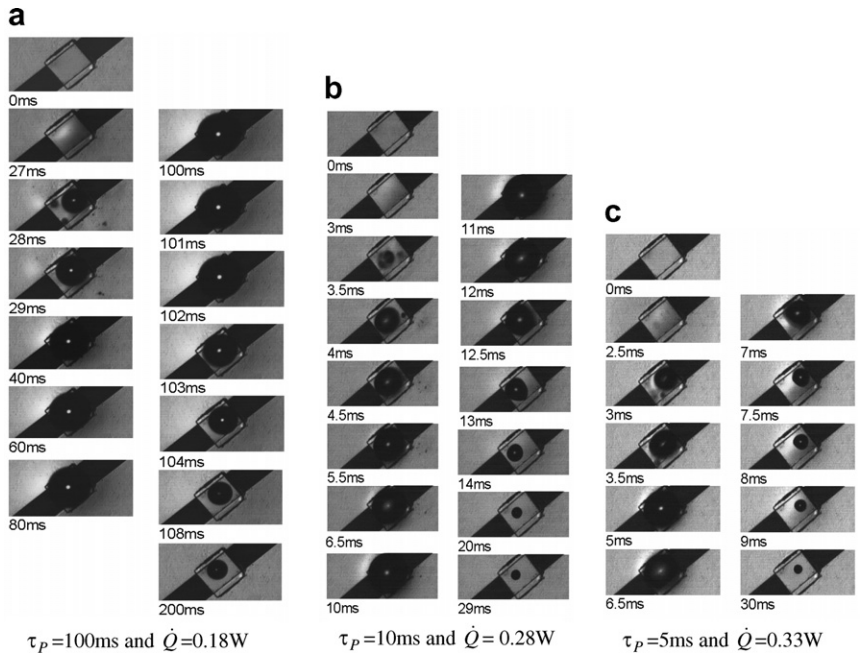

Fig. 3. Boiling incipience and bubble evolution during and after millisecond pulsed heating.

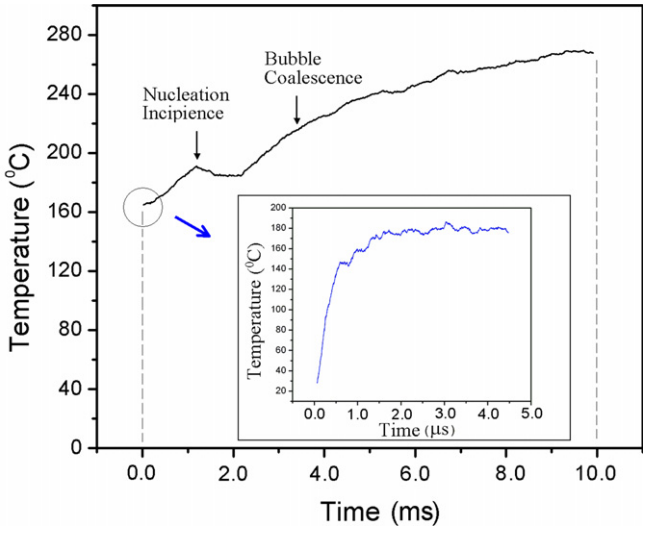

Fig. 4. A typical measurement of bulk temperature variation of the microheater during pulsed heating for $\tau_P = 10$ ms and $\dot{Q} = 0.28$ W.

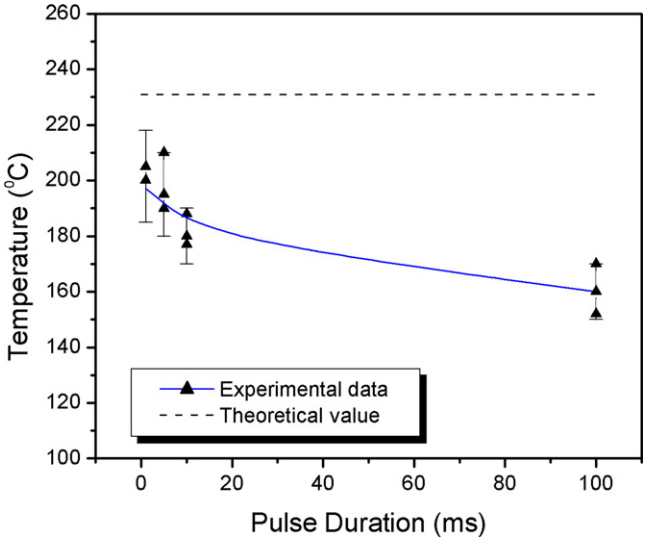

Fig. 5. Nucleation temperature for different pulse durations.

temperature for air-dissolved water as given by Li and Cheng [18],

$$T_{nl} - T_s = \frac{T_s \exp(C_g)}{h_{fg}\rho_v}\left(\sqrt{\frac{16\pi\sigma^3\omega}{3kT_{nl}\ln(N_0^{\gamma}kT_{nl}\psi/J\cdot h)}} - K_h C_g\right), \quad (1)$$

where C_g is the solubility of the dissolved gas and K_h is the Henry's constant, ψ is the surface available per unit bulk volume of liquid phase for heterogeneous nucleation, and ω is the geometric correction factor for the minimum work required to form a critical nucleus. For heterogeneous nucleation on a smooth surface with no cavities, these coefficients are given by $\psi = \frac{1}{2}(1+\cos\theta)$ and $\omega = \frac{1}{4}(1+\cos\theta)^2(2-\cos\theta)$. The solubility of air in water at 100 °C and 1 atm is 11.5×10^{-3} ml/ml and K_h is 155×10^6 Pa l/mole. As calculated from Eq. (1) (here $J = 1\ \mathrm{cm}^{-2}\ \mathrm{s}^{-1}$), the heterogeneous nucleation temperature of water with saturated dissolved air on a platinum smooth surface is determined to be approximately 231 °C with a contact angle of 20° (the detailed calculation process was given in [18]). As illustrated, there is significant variation in the magnitude of the experimental and theoretical values. There are several possible reasons for this comparatively large disparity, beside the fact that the present method

undershoots the highest temperature in the center of the microheater, including: (i) environmental noise, e.g., any unexpected external acoustic, electrical or magnetic fields; (ii) thermal stresses resulting from the microfabrication process and the pulsed heating; (iii) the possibility of contamination from nanoscale/submicron aliens (impurities) in water, which are invisible at 500× magnification, flowing over the heating surface occasionally; and (iv) the nanoscale/submicron defects on the surface of the platinum microheater. The first two of these could have a negative effect on the uncertainty of the experiments, when the high sensitivity of the temperature–resistance relationship of the microheater is considered, and the last two will decrease the nucleation temperature as indicated by the kinetics of boiling, respectively [18–22].

Figs. 6a–c illustrate the bubble evolution for a 100 ms, 10 ms and 5 ms heating pulses with respect to time, respectively. (The values in the parentheses in the figure legend, are the heat flux at the heating surface corresponding to the power levels.) It should be noted that the first large bubble to appear may, in reality, be the result of a number of smaller bubbles which have coalesced, but the process by which this occurs is so fast that it cannot be effectively resolved by the combination of the 500× optical microscope and the 2000 fps high-speed digital camera. From Fig. 6a, the bubble growth rate can be seen to be approximately 0.06 m/s and increases very slightly for higher pulse power levels. The initial acceleration of the bubble growth is on the order of 120–130 m/s^2 and is also related to the pulse power level, with higher pulse power levels resulting in slightly higher initial accelerations.

Similarly, Figs. 6b and c present the bubble dynamics for the 10 ms and 5 ms pulses, respectively. For the 10 ms pulse, the initial velocity is approximately 0.052–0.066 m/s and the initial acceleration is in the range of 100–130 m/s^2. For the 5 ms pulse, the initial velocity is approximately

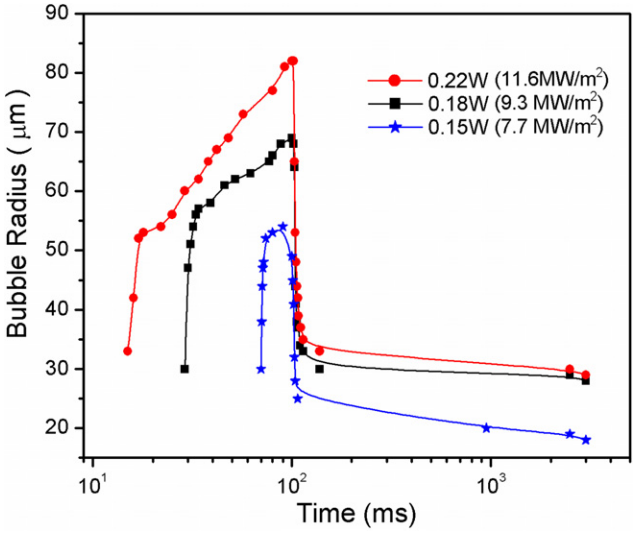

Fig. 6a. Bubble dynamics for 100 ms pulsed heating.

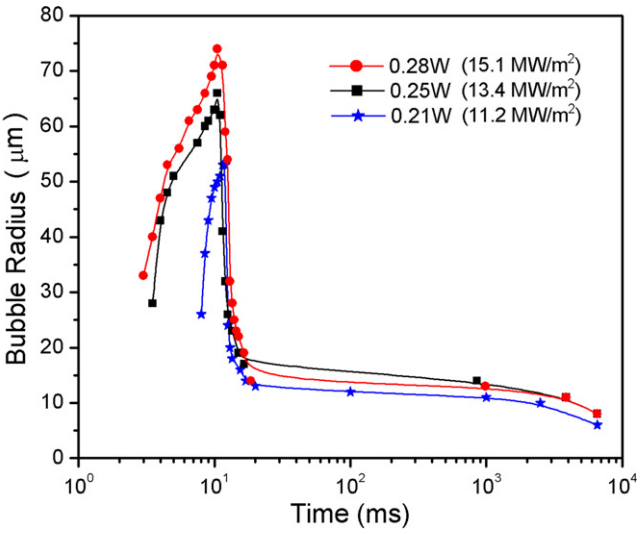

Fig. 6b. Bubble dynamics for 10 ms pulsed heating.

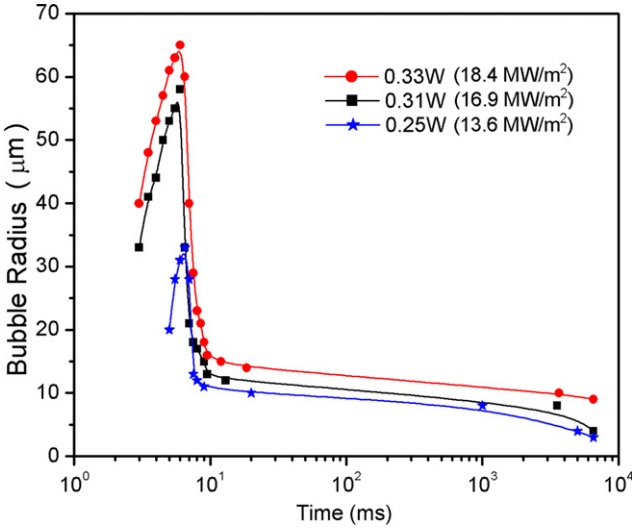

Fig. 6c. Bubble dynamics for 5 ms pulsed heating.

0.04–0.08 m/s and the initial acceleration is in the range of 80–165 m/s^2. From these results, it is apparent that the initial interface velocity and the initial interface acceleration are not only dependent on the pulse duration, but also highly dependent upon the intensity of the pulse power level (or the heating rate as used by other researchers). For a specific pulse duration, the higher the pulse power level, the higher the velocity and the acceleration; the shorter the pulse duration, the more apparent the dependence of the velocity and the acceleration on the pulse power level becomes.

A comparison of Figs. 6a–c indicates a number of common phenomena. First, in the early stages, the bubble growth occurs in two different stages: the first stage, which is very sharp, followed by a second stage in which the growth rate is slightly retarded, especially for large pulse

power levels. One explanation for this difference is the different controlling mechanism behind the bubble growth. At first, the non-equilibrium vapor pressure is the driving force (the dynamic stage), and later, the heat transfer from the heater and the ambient liquid becomes the driving force (the heat transfer stage), which is somewhat similar to the traditional depiction. In traditional bubble dynamics [23–25], for different stages controlled by different mechanisms, e.g., inertia stage, intermediate stage and thermal diffusion stage, a lot of simplifications were made to ease the problem, which is not proper for microscale pulsed heating situations. Generally, the Rayleigh–Plesset equation

$$R\ddot{R} + \frac{3}{2}\dot{R}^2 + 4\upsilon\frac{\dot{R}}{R} = \frac{1}{\rho_l}\left[P_v(R,t) - \frac{2\sigma}{R} - P_l(\infty,t)\right] \quad (2)$$

can be applied in any situation to describe the bubble growth with proper thermodynamic analysis of the vapor status inside the bubble and the heat and mass transfer around the interface. Since the mechanism behind the bubble evaluation under pulsed heating is not fully understood

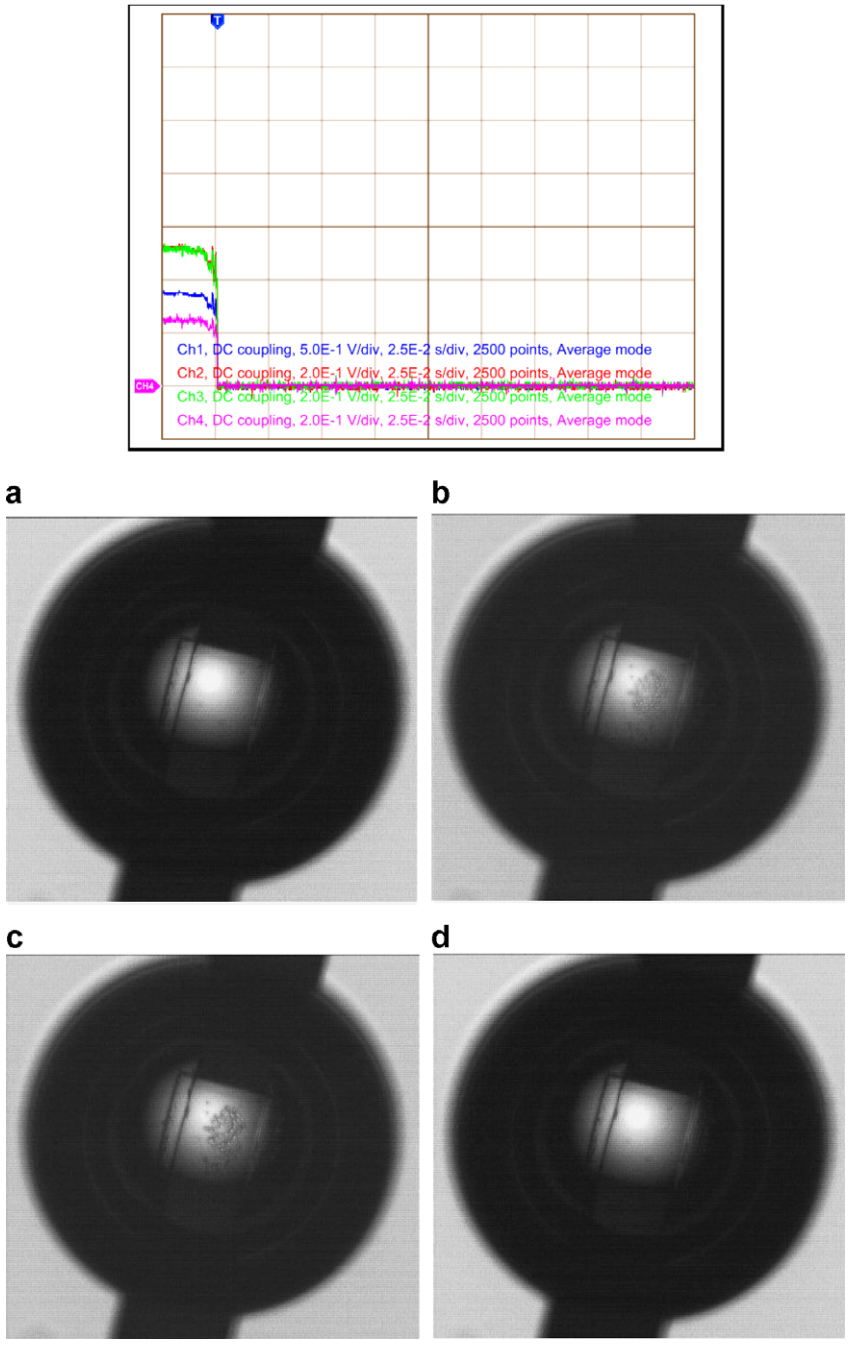

Fig. 7. Condensation phenomenon of vapor inside bubble on the surface of microheater after the sudden turnoff of the electrical current: (a) before the turnoff; (b) condensed droplets after the turnoff; (c) growth of the droplets; and (d) re-evaporation of the condensed droplets.

at this time, it is very hard to establish a well accepted theoretical model and more work must be done.

A second phenomenon common to all the experimental data is the sudden and rapid partial collapse of the bubble, immediately following the end of the pulse. A careful examination of the digital images shows that in each case, this sudden shrinkage began at a different time shortly after the termination of the pulse, e.g., 1.5 ms for a 5 ms pulse, ~3 ms for a 100 ms pulse, refer to Figs. 3a–c. This kind of time delay is a combination of two effects: one is the growth inertia from the previous growing stage before the end of the pulse; another one is the pressure decrease of the vapor inside the bubble due to the sudden cooling of the heater after the end of pulse. More experimental work is needed to identify this time delay for different pulse and different liquid bulk temperature.

This sudden intermediate shrinking of the bubble, which occurs near the end of the pulse, results mainly from the sudden decrease in the vapor pressure inside the bubble due to the decreasing temperature of the microheater cooled by the environmental water. In order to verify this estimation, further experimental observations were carried out. As shown in Fig. 7, if beforehand a big vapor bubble was generated with a quasi-steady state heating method as shown in Fig. 7a, and the electrical current was suddenly turned off, through the high-speed CCD camera, a very interesting phenomenon was observed: several tiny condensed droplets appeared on the central surface of the microheater (Figs. 7b–c). This kind of phenomenon clearly demonstrated that the microheater is cooled by the connection pads and the surrounding cold liquid after the heating pulse. Also this cooling effect has a significant influence on the vapor pressure inside the bubble causing the sudden collapse for the pulsed heating situations, due to the high degree of sub-cooling of the liquid. It should be noted that for the above experiment, since it was near saturation boiling for a quasi-steady heating process, even after the elimination of the electrical current, the bubble did not shrink. In addition, since the temperature drop of the microheater was so small and the heat from the ambient liquid quickly compensated for this drop, it appears that the evaporation of the condensed droplet as shown in Fig. 7d compensates.

Further experiments clearly indicate that if the heating pulse is short enough. e.g., $\leqslant$5 ms, the dynamic stage of bubble growth is directly followed by the sudden shrinkage and the heat transfer stage of bubble growth never occurs. This phenomenon may account for the observations of Asai, which indicated a parabolic form of bubble growth and collapse under microsecond pulsed heating [1].

Fig. 8 presents the maximum measured bubble radius as a function of the pulse duration and power level. In order to be consistent with classical analyses [1,11,15], the heat flux at the heated surface is presented as one of the pulse parameters. The results indicate that for certain pulse durations, the maximum bubble radius is directly related to the heat flux. The reason for a larger maximum bubble radius for longer pulsed heating is that the comparatively longer

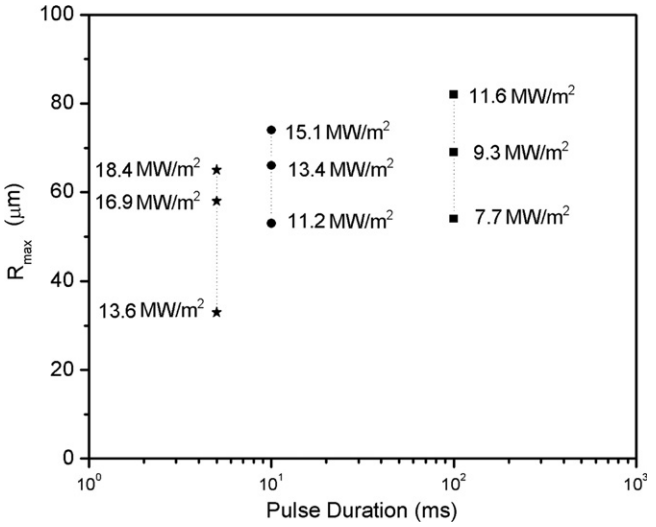

Fig. 8. Maximum bubble radius for different pulse durations and power levels.

heat transfer stage results in a greater total energy input, and hence, a larger final bubble radius. This information is useful for future bubble dynamics modeling and in particular, for the design of the thermal actuated MEMS.

For certain pulse durations, increases in the total pulse power level beyond a certain value, result in a situation in which the heating is so rapid that small nucleate bubbles can not merge into a single larger bubble. As depicted in Fig. 9, the small nucleate bubbles will strike against each other and be effectively pushed away from the heating surface and each other. This phenomenon is referred to as "*bubble splash*". The reason for this *bubble splash* may be that the initial non-equilibrium vapor pressure is quite high and the number of nucleate bubbles is very large for the higher pulse power levels [26]. Thus, perturbations generated from the bubble nucleation and growth increase with increases in the pulse power level. If the force resulting from this violent non-equilibrium explosive boiling is not relaxed or reduced through bubble growth, the neighboring bubbles will be pushed away and resemble a splash of bubbles. By repeating the experiments with an incremental increase of 0.2 V, the range over which bubble combination and bubble splash occurred can be identified, as shown in Fig. 10. The two curves illustrated in Fig. 10 represent the boundaries for bubble formation and growth. If the heat flux at the surface is below the lower curve, there will be no bubble formation or bubble coalescence, and if the heat flux at the surface is higher than the upper curve, *bubble splash* will be the dominant occurrence. Ideally, the preferable range for the application of bubble actuation is located in the region between these two curves.

5. Conclusions

Quantitative results for transient boiling occurring on smooth surfaces under millisecond pulsed heating were pre-

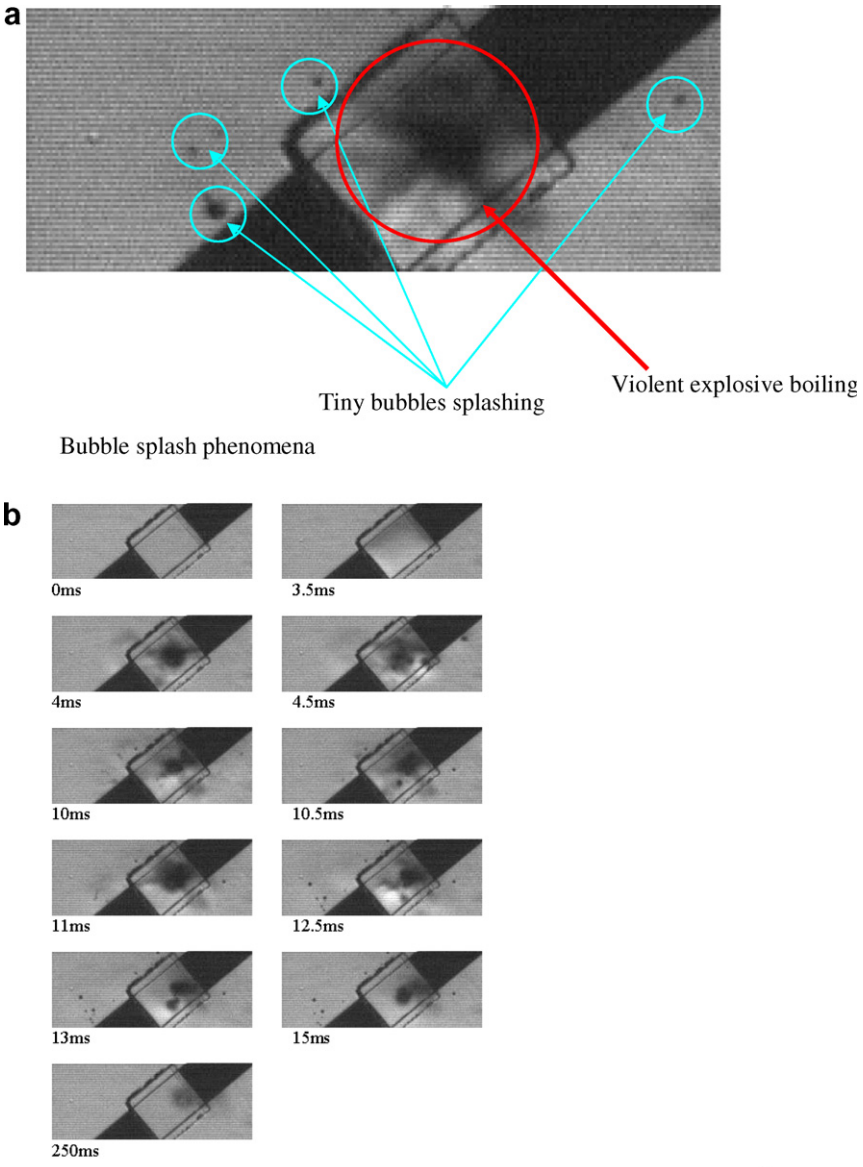

Fig. 9. Violent explosive boiling and bubble splash under high power pulsed heating.

sented and discussed. A number of conclusions can be drawn from the present studies. By measuring both the power variations and the temperature variations during pulsed heating and transient boiling on a platinum microheater, it is apparent that the shorter the pulse durations and the higher the pulse power levels, the closer the nucleation temperature is to the theoretical value.

It was clearly apparent from these tests and the analysis of the results, that the maximum bubble radius is dependent not only on the heat flux on the surface, but also on the pulse duration, with the end of the pulse resulting in a sudden partial bubble collapse, due to the cooling of the ambient liquid and the sudden decrease in the vapor pressure inside the bubble. In addition, the bubble growth from a smooth surface was found to exhibit characteristic behavior and occur in two distinct stages, a dynamic stage and a heat transfer stage, the duration of which depends on the transient heating process. Finally, it appears that if the heating rate is sufficiently high (or the pulse power level is sufficiently high for a specific pulse duration), a phenomenon referred to as *bubble splash* will occur, in which small individual bubbles will not coalesce into a single larger bubble, due to the high non-equilibrium vapor pressure inside the bubble nuclei.

The information provided in this work can help in the design of the thermal bubble actuated MEMS applications, e.g., the suitable pulse parameters can be inferred for the effective bubble actuation from the present work, and the preferred pulse parameters can be obtained with the aid of the bubble dynamics study.

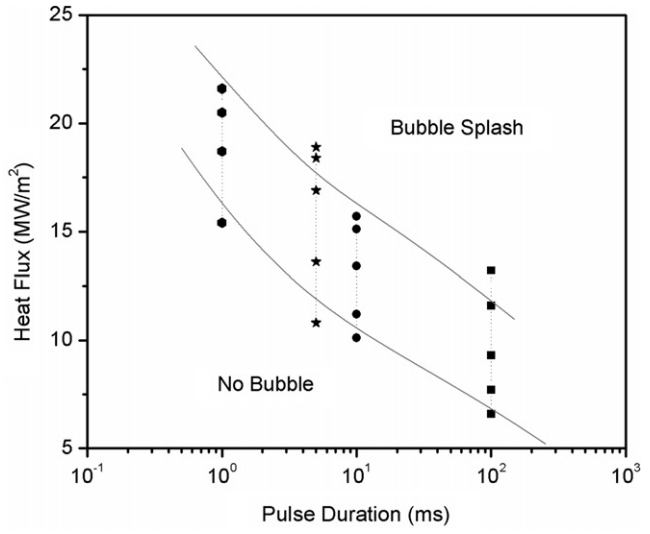

Fig. 10. Stable zone for bubble coalescence and growth for different pulse durations.

Acknowledgements

This work was supported by the Office of Naval Research Grant ONR N000140010454. The third author (P. Cheng) wishes to thank the National Natural Science Foundation of China for partial support of this work through Grant No. 50536010.

References

[1] A. Asai, Bubble dynamics in boiling under high heat flux pulse heating, ASME J. Heat Transfer 113 (1991) 973–979.
[2] H. Yuan, H.N. Oğuz, A. Prosperetti, Growth and collapse of a vapor bubble in a small tube, Int. J. Heat Mass Transfer 42 (1999) 3643–3657.
[3] X. Geng, H. Yuan, H.N. Oguz, A. Prosperetti, Bubble-based micropump for electrically conducting liquids, J. Micromech. Microeng. 11 (3) (2001) 270–276.
[4] T. Okamoto, T. Suzuki, N. Yamamoto, Microarray fabrication with covalent attachment of DNA using bubble jet technology, Nat. Biotechnol. 18 (4) (2000) 438–441.
[5] J. Tsai, L. Lin, Active microfluidic mixer and gas bubble filter driven by thermal bubble micropump, Sensor. Actuator. A 97–98 (2002) 665–671.
[6] R.B. Maxwell, A.L. Gerhardt, M. Toner, M.L. Gray, M.A. Schmidt, A microbubble-powered bioparticle actuator, IEEE/ASME J. Microelectromech. Syst. 12 (5) (2003) 630–640.
[7] J.R. Lindner, Microbubbles in medical imaging: current applications and future directions, Nat. Rev. Drug Discov. 3 (6) (2004) 527–532.
[8] P.G. Deng, Y.K. Lee, P. Cheng, Measurements of micro bubble nucleation temperatures in DNA solutions, J. Micromech. Microeng. 15 (3) (2005) 564–574.
[9] Y.K. Lee, U.C. Yi, F.G. Tseng, C.J. Kim, C.M. Ho, Fuel injection by a thermal microinjector, in: Proc. MEMS (MEMS – Vol. 1), ASME Int. Mechanical Engineering Congress and Exposition, Nashville, TN, 1999, pp. 419–425.
[10] L.W. Lin, Microscale thermal bubble formation: thermophysical phenomena and applications, Microscale Thermophys. Eng. 2 (2) (1998) 71–85.
[11] Y. Iida, K. Okuyama, K. Sakurai, Boiling nucleation on a very small film heater subjected to extremely rapid heating, Int. J. Heat Mass Transfer 37 (17) (1994) 2771–2780.
[12] C.T. Avedisian, W.S. Osborne, F.D. McLeod, C.M. Curley, Measuring bubble nucleation temperature on the surface of a rapidly heated thermal ink-jet heater immersed in a pool of water, Proc. Roy. Soc. Lond. Ser. A – Mathemat. Phys. Eng. Sci. 455 (1991) (1999) 3875–3899.
[13] O.C. Thomas, R.E. Cavicci, M.J. Tarlov, Effect of surface wettability on fast transient microboiling behavior, Langmuir 19 (2003) 6168–6177.
[14] Z. Zhao, S. Gold, D. Poulikakos, Pressure and power generation during explosive vaporization on a thin-film microheater, Int. J. Heat Mass Transfer 43 (2000) 281–296.
[15] Z. Yin, A. Prosperetti, J. Kim, Bubble growth on an impulsively powered microheater, Int. J. Heat Mass Transfer 47 (2004) 1053–1067.
[16] P.G. Deng, Y.K. Lee, P. Cheng, The growth and collapse of a microbubble under pulse heating, Int. J. Heat Mass Transfer 46 (2003) 4041–4050.
[17] J. Li, G.P. Peterson, Microscale heterogeneous boiling on smooth surface? from bubble nucleation to bubble dynamics, Int. J. Heat Mass Transfer 48 (2005) 4316–4332.
[18] J. Li, P. Cheng, Bubble cavitation in a microchannel, Int. J. Heat Mass Transfer 47 (2004) 2689–2698.
[19] Y. Hsu, On the size range of active nucleation cavities on a heating surface, ASME J. Heat Transfer 84 (1962) 207–216.
[20] R. Cole, Boiling nucleation, Adv. Heat Transfer 10 (1974) 86–166.
[21] V.P. Skripov, Metastable Liquids, John Wiley & Sons, New York, 1974.
[22] C.T. Avedisian, The homogeneous nucleation limits of liquids, J. Phys. Chem. Ref. Data 14 (3) (1985) 695–729.
[23] B.B. Mikic, W.M. Rohsenow, P. Griffith, On bubble growth rates, Int. J. Heat Mass Transfer 13 (1970) 657–666.
[24] A. Prosperetti, M.S. Plesset, Vapour-bubble growth in a superheated liquid, J. Fluid Mech. 85 (Part 2) (1978) 349–368.
[25] H.S. Lee, H. Merte Jr., Spherical bubble growth in liquids in uniformly superheated liquids, Int. J. Heat Mass Transfer 39 (12) (1996) 2427–2447.
[26] J. Li, G.P. Peterson, P. Cheng, Mechanical non-equilibrium consideration of homogeneous bubble nucleation for an unsteady-state boiling process, Int. J. Heat Mass Transfer 48 (15) (2005) 3081–3096.